JANUARY 1981

PPPL-1676
UC-20f



# FAST-WAVE HEATING IN THE TWO-ION HYBRID REGIME ON PLT

## PLASMA PHYSICS LABORATORY

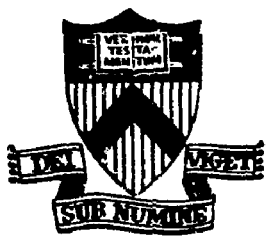




PRINCETON UNIVERSITY
PRINCETON, NEW JERSEY

This work was supported by the U.S. Department of Energy Contract No. DE-AC02-76-CHO 3073. Reproduction, translation, publication, use and disposal, in whole or in part, by or for the United States government is permitted.

# Fast-Wave Heating in the Two-Ion Hybrid Regime on PLT

D. Q. Hwang, R. E. Chrien, P. Colestock, S. L. Davis,
R. J. Goldston, J. C. Hosea, H. Hsuan, R. Kaita,
S. Medley, D. Mueller, J. D. Strachan, S. Suckewer,
H. R. Thompson, and G. Zankl*
Plasma Physics Laboratory, Princeton University
Princeton, New Jersey 08544 USA

## ABSTRACT

Plasma heating using the fast magnetosonic wave in the ion cyclotron range of frequencies is being studied both experimentally and theoretically in order to evaluate its potential for heating reactor plasmas. RF pulses at power levels up to 800 kW and length >130 ms have been delivered to a set of two parallel 1/2 turn loop antennae with 80% of the power coupled to the plasma. The parallel antennae have been driven both in and out-of-phase so that the $k_\phi$ dependence of the antenna coupling and plasma heating can be determined. The heating experiments were conducted in the two-ion hybrid regime where the deuterium plasma contained a small component of a second ion species (hydrogen or $^3$He). A bulk ion temperature increase of up to 1.2 keV has been achieved at the 620 kW power level with $^3$He as the minority species and $\bar{n}_e = 2.9 \times 10^{13}$ cm$^{-3}$. Energetic minority distributions have been detected consistent with theory.

---

*Permanent address: Max-Planck-Institut für Plasmaphysik.

## I. Introduction

RF heating in the ion cyclotron range of frequencies (ICRF) has met with considerable success in producing ion heating in the first generation of tokamaks (ST, TO-1, ATC, TFR)[1-4]; however, many questions concerning the precise nature of the heating mechanism, its scaling to reactor plasmas, and other observed effects on the plasma, such as electron density increases and impurity influx, still remain unanswered. It is expected that ion heating efficiency should improve and at the same time deleterious effects on the plasma should decrease in the larger and higher current devices. This scaling has, in fact, been borne out in recent ICRF experiments in PLT where efficient, centrally peaked ion heating has been achieved with minimal degradation of the discharge quality.

Until recently the high power ICRF experiments on PLT have been conducted on the two-ion hybrid regime (24.6 MHz). A higher frequency system (42 MHz) has recently been completed which will allow study of pure second harmonic heating as well as minority heating at higher toroidal fields. The single 1/2 turn loop antenna used in previous experiments has been replaced by two 1/2 turn loops connected in parallel so that high power can be applied and better control over the excited $k_\phi$ spectrum can be obtained. This paper is focused chiefly on the results in the two-ion hybrid regime.

In the two-ion hybrid regime, the wave energy is preferentially coupled to the minority species where the power per particle can be high, creating a very energetic ion distribution

which equilabrates with the background electrons and ions. The confinement of these energetic ions, as in neutral beam heating, is important to the heating efficiency and can be tested in PLT where the plasma current is comparable to that in the next generation of tokamaks.

In Section II the theory of wave absorption in the two-ion hybrid regime is discussed based on a one-dimensional, hot-plasma model. Recent heating data using two parallel coils are presented in Section III. A preliminary calculation of power balance using the theoretical power deposition model is presented and compared to the experiment in Section IV. Finally, conclusions concerning the scaling of ICRF heating to reactors based on the experimental results and the self-consistent wave theory is presented in Section V.

## II. Two-Ion Hybrid Theory

The effects of the two-ion hybrid layer on fast wave propagation in tokamaks have been observed experimentally on the ATC and TFR tokamaks and theoretically treated by Swanson, Perkins, Jacquinot, and others.[5-10] For a finite temperature plasma with weak minority concentration, most of the absorbed wave power is predicted to couple directly to the minority ions through fundamental cyclotron damping in the so-called direct minority damping regime. When the concentration of the minority is sufficiently high, the fast wave can couple to an ion Bernstein wave via mode conversion. Depending on the $k_{\parallel}$ spectrum the mode converted wave can lead to electron Landau damping or

majority second harmonic heating if the layer is present in the plasma.

The minority concentration, $\eta = zn_i/n_e$, necessary for mode conversion to occur has previously been reported to be

$$\eta_h \geq \left(\frac{\beta_e T_h}{2T_e}\right)^{1/2} s_{\parallel}\left(\frac{4}{3} + s_\phi^2\right) \qquad (1)$$

where $s = kc/\omega_{pd}$, and $k_{\parallel}$ and $k_\phi$ are the wave numbers along the total and toroidal magnetic field directions, respectively.[8] However, when compared with the full hot plasma dispersion relation, it is found that the mode conversion concentration is also an inverse function of bulk ion density and occurs even for zero minority concentration. An approximate hot plasma dispersion relation for the fast wave and Bernstein wave in this parameter regime, without rotational transform ($n_{\parallel} << n_{\perp}$) is given by $K_{xx}(n_{\perp}^2 - K_{yy}) + K_{xy}^2 = 0$ where $K_{xx}$, $K_{yy}$, $K_{xy}$ are the components of the hot plasma dielectric tensor.[11] Using the full hot plasma dispersion relation, the mode conversion onset condition for various densities is compared with the previous estimate Eq. (1), in Fig. 1.

Since a Bernstein wave can exist between any pair of harmonic cyclotron frequencies for $n_{\perp} >> n_{\parallel}$, there can be a mode conversion between the fast wave and the Bernstein wave at any minority concentration for sufficiently high density. Since the Bernstein wave is a function of the temperature, the precise nature of the wave dispersion is sensitive to the t perature

profile. Figure 2 shows the mode conversion between the deuteron and triton second harmonics in a D-T plasma. Temperature profile effects are included, where an additional mode conversion can occur, impeding fast wave penetration to the plasma core. Thus this accessibility condition requires that a minimum allowable $k_{\parallel}$ value be excited.

When the cyclotron layer occurs near the two-ion hybrid layer (low concentration or high temperature), the tunneling, reflection, and absorption coefficients have to be modified; this problem has not been treated in detail theoretically except for some recent work by Swanson.[12] We have developed a numerical algorithm to solve for the fields based on a one-dimensional hot plasma wave operator. Neglecting corrections to the conductivity of order $r_L/R$ where $r_L$ is the Larmor radius and R is the major radius, the full wave solution can be found by dividing the domain into thin, uniform slabs within which the solution can be written as a sum of individual wave components of the form

$$E_y = \sum_{i=1}^{4} \epsilon_i \, e^{ik_{xi}x} \quad . \tag{2}$$

Energy is conserved by requiring that the Poynting flux is continuous across slab boundaries. The scattering matrix for the problem is obtained by multiplying the 4 × 4 matrix for each individual slab; mode conversion coefficients are then determined through elimination by imposing boundary conditions appropriate for high or low field side incidence. Once these

coefficients are known, the total E-field within the absorption zone can be constructed.

The dispersion relation and the resulting full wave solution for the case of low field incidence are shown in Fig. 3(a) and 3 (b). Very little wave power tunnels through the relatively thick evanescent zone; however, the reflection coefficient is also small due to tne effective double pass damping through the cyclotron layer primarily by the minority protons. This case is typical for the parameter range in the current PLT experiments and indicates that minority species heating should dominate over majority second harmonic and electron Landau damping.

## III. Experimental Results

The antenna structure used in the recent ICRF heating experiments in PLT consists of two 1/2 turn loops connected in parallel and placed 45 cm apart in the toroidal direction. The antennae are driven at either 0° or 180° relative phase which gives rise to a toroidal mode spectrum centered about N=0 or N=9, respectively ($k_\phi$ = N/R where R is the major radius). For the spectrum centered about N=0, the plasma loading is a sensitive function of the electron density due to onset conditions while the spectrum centered about N=9 shows little density dependence for sufficiently strong damping. In order to maintain constant antenna loading, most of the high power experiments were carried out with out-of-phase drive. The oscillator frequency is 24.6 MHz which places the fundamental cyclotron layer for hydrogen or the fundamental cyclotron layer for $^3$He on the axis of the machine

at toroidal magnetic fields of 16 and 24 kG, respectively. Up to 300 kW of constant rf power has been delivered to the coils for a pulse duration >130 ms with 80% of this power coupled to the plasma. Typical PLT discharge parameters are given by $\bar{n}_e = 2\text{-}4 \times 10^{13}$ cm$^{-3}$, $T_i(0) = 500\text{-}800$ eV, $T_e(0) = 1\text{-}1.5$ keV, $V_\phi = 1.3$ V, $Z_{eff} = 2\text{-}3$, and $I_p = 230\text{-}450$ kA.

Similar to results previously reported in the single coil excitation experiments in D-H plasma,[13-15] an energetic hydrogen distribution, isotropic up to 40 keV, with an effective temperature of >7 keV has been measured in two coil operation using a mass selective perpendicular charge exchange system.[14] The measured distribution agrees well with the isotropic Fokker-Planck theory, including a quasilinear rf diffusion operator.[16] Heating efficiency for the deuterium plasma with hydrogen minority is shown in Fig. 4 where the deuterium temperature increase on axis, $\Delta T_d(0)$, is plotted against $P_{rf}/n_e$ and is found to be nearly linear with a slope of 3 eV/kW (normalized to $1 \times 10^{13}$ cm$^{-3}$). When $^3$He is used as the minority species, the heating efficiency is nearly double that of the hydrogen minority case due to stronger ion-ion coupling between $^3$He and the bulk deuterons and the comparatively lower charge exchange losses of the doubly ionized $^3$He ions. Moreover, for the $^3$He case, higher toroidal magnetic fields are used which permit higher current discharges (400-450 kA) to be obtained in PLT leading to better confinement of the energetic ions as observed in previous experiments.[14]

Although the energy distribution of the $^3$He minority has not been directly measured due to the low charge exchange cross section of the $^3$He ion, the existence of energetic $^3$He particles has been confirmed by activation measurement of 14 MeV protons produced by the D($^3$He,p)$\alpha$ reaction. Samples of titanium are activated by proton capture, $^{48}$Ti[p(>10 MeV),n]$^{48}$V, producing a $^{48}$V nucleus which is detected by $\gamma$-decay at 1.312 MeV and 0.983 MeV with a 16 day half-life. From the level of activity measured from the samples, the D-$^3$He reaction is of the order of $10^{12}$/sec which is a large fusion production comparable to the D(d,n)$^3$He rate produced by 40 keV deuterium neutral beam injection. The large number of D-$^3$He reactions can be accounted for by the energy sensitive reaction cross section ($\propto W_{^3He}^6$), confirming the existence of an energetic minority tail.

The highest bulk deuteron temperature achieved with rf heating in a D-$^3$He plasma is about 2 keV with $P_{wave}$ = 620 kW at $\bar{n}_e = 2.9 \times 10^{13}$ cm$^{-3}$. Figure 5 shows the neutron emission averaged over a series of discharges where the neutron flux increased by a factor of $2 \times 10^2$ during the rf pulse, and the deuteron temperature deduced from the neutron emission data indicated at $\Delta T_d(0)$ of 1 keV. $Z_{eff} = 1$ has been assumed in this temperature estimate from neutron flux so it represents a lower limit on $\Delta T_d(0)$. A high resolution neutron energy spectrum was measured using a $^3$He neutron spectrometer by averaging over a large number of rf heated discharges and is shown in Fig. 6. A well defined peak at 2.45 MeV corresponds to D-D reactions and is sufficiently narrow that its width could be

determined by the Doppler broadening of a Maxwellian, indicating a thermonuclear neutron origin.[17] The deuteron temperature is independently measured by a mass sensitive charge exchange system and found to be in good agreement with the neutron data (Fig. 7). (In this measurement high density corrections have not been taken into account so this $\Delta T_d(0)$ is a lower limit.) Moreover, the neutron flux, measured by a toroidal array of In activation foils, is found to be toroidally uniform, thus indicating that the neutron emission is not localized at the rf coils by trapped particle or near field effects.

The ion temperature profile obtained from Doppler broadening of impurity lines and the radially scanning charge exchange system is shown in Fig. 8 for a D-$^3$He discharge. The ion temperature profile is quite broad out to 15 cm which is consistent with the theoretically calculated power deposition profile for the rf wave.

The radiation profile during rf heating is obtained using bolometers and spectroscopy in order to determine the impurity influx from the wall and limiters. During the rf pulse, the radiation profile becomes more centrally peaked, indicating some influx of heavy impurities such as Fe and Ti as seen by spectroscopic measurements, and the total amount of radiation is more than can be accounted for by the electron density increase due to the rf pulse. The total volume integrated power during the rf pulse is 55% of the ohmic power plus rf power. The impurity influx is substantially smaller at higher ohmic currents where energetic ion confinement is better or at higher densities

where energetic ion confinement is better or at higher densities where the mean minority ion energy is smaller.

## IV. Power Balance

Ion power balance using experimental parameters corresponding to specific heating cases in both D-H and D-$^3$He regimes, has been calculated using a one-dimensional model. The theoretical rf power deposition profiles are obtained by an iterative scheme based on geometric optics. The incident wave from the distributed source is centrally peaked due to geometric focusing. The total absorbed power and the equipartition among species is found using the full-wave slab model described earlier. The power deposition profile thus determined is used to calculate the minority species distribution using Fokker-Planck theory as given by Stix. The wave absorption calculation is iterated using the non-Maxwellian distributions leading to a further enhancement of the predicted single-pass absorption into the minority species.

The energetic minority distribution plus the rf power coupled directly to the deuterium wave serve as the inputs to the ion power balance. The ion power balance equation is given as follows

$$\frac{\partial E_i}{\partial t} = Q_{ei} + Q_{tc} + Q_{pd} + Q_{cx} + Q_{rf}$$

where $E_i$ is the ion energy content, $Q_{ei}$ is the energy exchange between electrons and ions, $Q_{tc}$ is the neoclassical thermal

conduction, $Q_{pd}$ is the energy change associated with particle diffusion, $Q_{cx}$ is the energy loss due to charge exchange and ionization, and $Q_{rf}$ is the power input to the deuterons from the sources mentioned above. In the calculation, measured values for the electron temperature and density provided by Thomson scattering and microwave interferometry measurements are assumed. The ion temperature profiles calculated by the code are compared with Doppler broadening measurements.

Figure 9 shows the ion power balance for the D-H plasma where the rf power input is 350 kW. The power per particle delivered to the minority ions is high enough so that the resulting energetic minority distribution couples a substantial fraction of the power (190 kW) to the electrons through electron drag; however, there is no electron heating observed experimentally in this case. The experimental temperature stayed constant and the lack of electron heating may be explained by the increase in the radiation level during the rf pulse as shown in Fig. 8. In other cases, particularly when the impurity flux was lower, substantial electron heating was observed.

For the D-$^3$He plasma, shown in Fig. 9, the input power is lower (150 kW). In this plasma, the minority species couples more strongly to the background plasma resulting in a less energetic distribution and thus stronger coupling to the majority ion species relative to the electrons. In this case almost all of the energy from the minority distribution is coupled to the deuterium with only 30 kW going to the electrons. Furthermore, there is little charge exchange loss for $^3$He due to the lower

charge exchange cross section for the doubly charged ions. The power balance calculations for both the D-H and D-$^3$He cases are in good agreement with experiment and are consistent with the experimentally observed higher heating efficiency for the $^3$He minority case.

## V. Conclusions and Scaling

A number of conclusions can be drawn from the good agreement between theory and experiment in these recent PLT experiments. According to the full wave theory, minority absorption of the wave power dominates even well into the mode conversion regime when the wave is launched from the low field side and this is observed to be the case in PLT. As seen from the heating results, confinement of energetic minority ions is crucial for fast wave heating in the two-ion hybrid regime. Thus, in PLT, as in the next generation of tokamaks, efficient wave heating should be possible. Moreover, the minority distribution can be controlled by varying the electron density or the minority density so that minority ion energy can be preferentially coupled either to the bulk ions or electrons. Furthermore, $Z > 1$ minority species can be used for better ion-ion coupling and lower charge exchange losses leading to higher heating efficiency. The capability of producing an energetic $Z > 1$ ion distribution in the plasma with rf heating can be useful for future advanced fuel reactors.

## ACKNOWLEDGMENTS

The authors wish to thank the PPPL Engineering Support Staffs for their valuable contributions to this program and Drs. F. Perkins, T. Stix, J. Jacquinot, J. Adam, and G. Swanson for helpful discussions of the theory. This work was supported by U. S. DOE Contract No. DE-AC02-76-CHO-3073.

REFERENCES

[1]The ST Group, in Plasma Physics and Controlled Nuclear Fusion Research (Proc. 5th Int. Conf., Tokyo, Japan, 1974) Vol. I, IAEA, Vienna (1975) 65.

[2]V. L. Vdovin and N. V. Shapotkovskii, Proceedings 3rd International Meeting on Theoretical and Experimental Aspects of Heating of Toroidal Plasmas, Vol. II (1976) 349.

[3]H. Takahashi, C. C. Daughney, R. A. Ellis, R. J. Goldston, H. Hsuan, T. Nagashima, F. J. Paoloni, A. J. Sivo, and S. Suckewer, Phys. Rev. Lett. 39 (1977) 31.

[4]TFR Equipe, Proceedings 3rd International Meeting on Theoretical and Experimental Aspects of Heating of Toroidal Plasmas, Vol. I (1976) 87.

[5]S. F. Buchsbaum, Phys. Fluids 3 (1960) 418.

[6]D. G. Swanson, Phys. Rev. Lett. 36 (1976).

[7]F. W. Perkins, Nucl. Fusion 17 (1977) 1197.

[8]J. Jacquinot, B. D. McVey, and J. E. Scharer, Phys. Rev. Lett. 39 (1977) 38.

[9]V. L. Vdovin, N. N. Shapotkovskii, and A. V. Chesnikow, Proceedings 8th European Conference on Controlled Fusion and Plasma Physics, Vol. I (1978) 19.

[10]H. Takahashi, Journal de Physique 38 (1977) 171.

[11]T. H. Stix, The Theory of Plasma Waves, Chapter 9 (1962).

[12]D. G. Swanson, Phys. Fluids 21 (1978) 926.

[13]P. L. Colestock et al., Proceedings Joint Varenna-Grenoble International Symposium on Heating in Toroidal Plasmas, Vol II (1978) 217.

[14]J. C. Hosea et al., "Fast Wave Heating in the Princeton Large Torus", PPPL-1588 (1979).

[15]D. Hwang et al., Proceedings 9th European Conference on Controlled Fusion and Plasma Physics, Oxford, paper B-2.7 (1979).

[16]T. Stix, Nucl. Fusion 15 (1975) 737.

[17]J. D. Strachan et al., Nature 279 (1979) 626.

FIGURE CAPTIONS

Fig. 1. Minimum minority concentration for mode conversion onset. (PPPL803426)

Fig. 2. Mode conversion between the triton and deuteron second harmonic at high density due to the temperature profile $n_e(0) = 1 \times 10^{15}$ cm$^{-3}$, $T_d = T_t = T_o \left[1 - (r/a)^2\right]^2$. (PPPL803450)

Fig. 3. (a) Dispersion relation roots for the case of $n_e(0) = 4 \times 10^{13}$, $T_e(0) = 2$ keV, $n_p = 10\%$, $T_d(0) = 2$ keV, $T_p(0) = 7$ keV, $K_{\parallel} = 5$ m$^{-1}$, $B_T = 17.7$ kG, f = 25 MHz. (b) Corresponding wave components of the full wave solution for low field incidence. $P_{tr} = 5\%$, $P_{ref} = 18\%$, $P_{abs}(min) = 75\%$, $P_{abs}(maj) = 2\%$.

Fig. 4. Deuteron temperature increase vs. normalized wave power. (PPPL803428)

Fig. 5. Neutron emission and deduced central deuteron temperature ($Z_{eff} = 1$ is assumed). (PPPL803429)

Fig. 6. High resolution neutron energy spectrum during rf heating. (PPPL803431)

Fig. 7. Perpendicular CX measurements of deuteron temperature during rf heating. (PPPL803433)

Fig. 8. (a) Radial ion temperature profile obtained from spectroscopic measurements. (b) Total volume integrated radiation losses for ohmic and ohmic + rf heated cases.

Fig. 9. Ion power balance for (a) D-H and (b) D-$^3$He rf heated plasmas. (PPPL803425, PPPL803432)

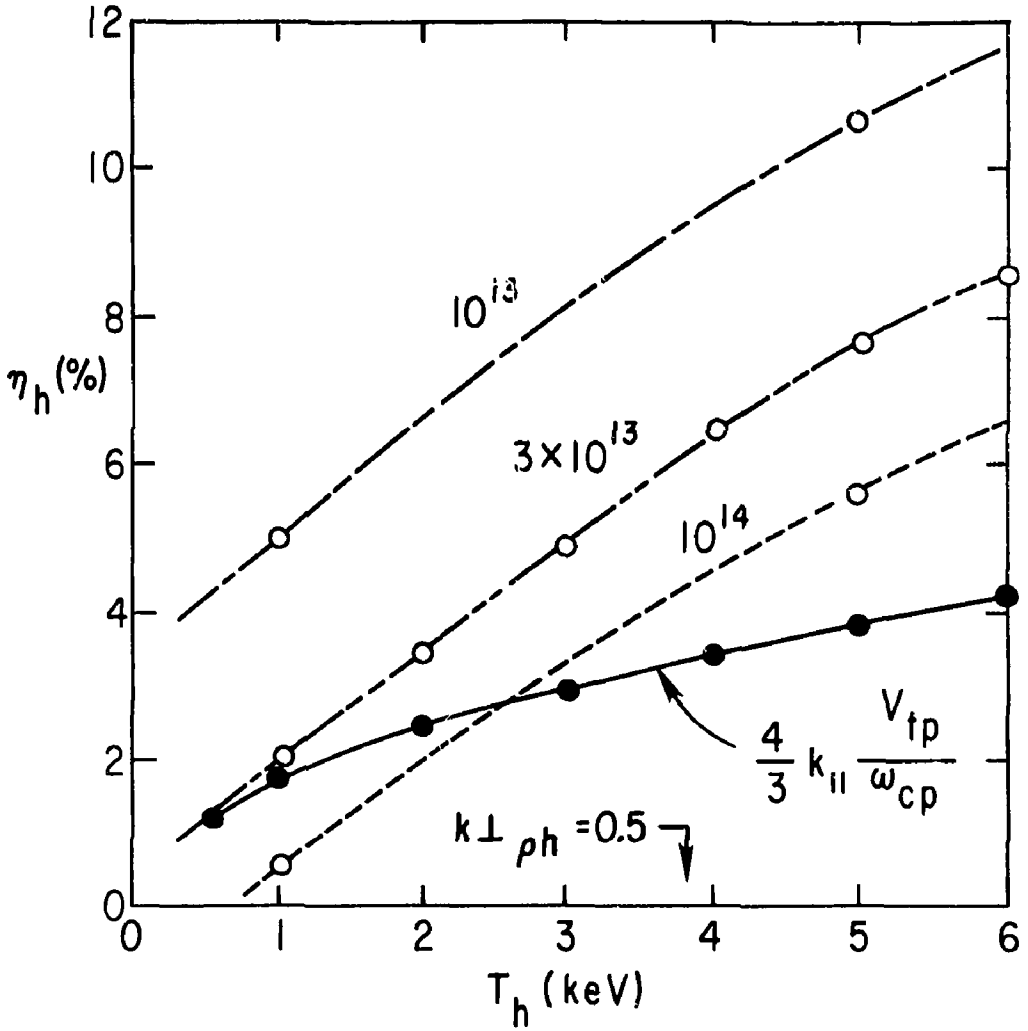


Fig. 1. (PPPL-803426)

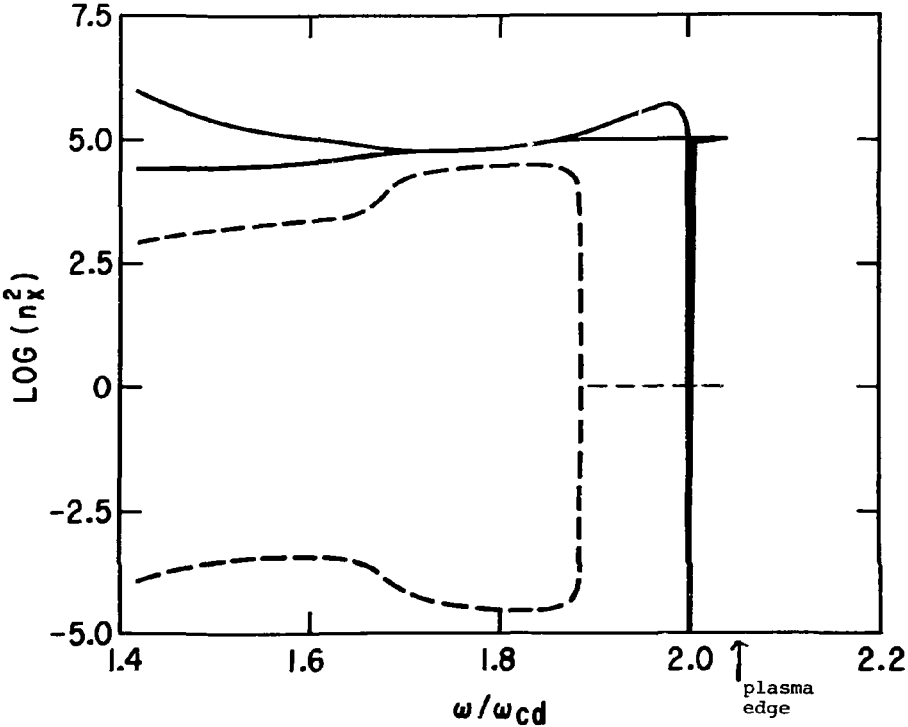


Fig. 2. (PPPL-803450)

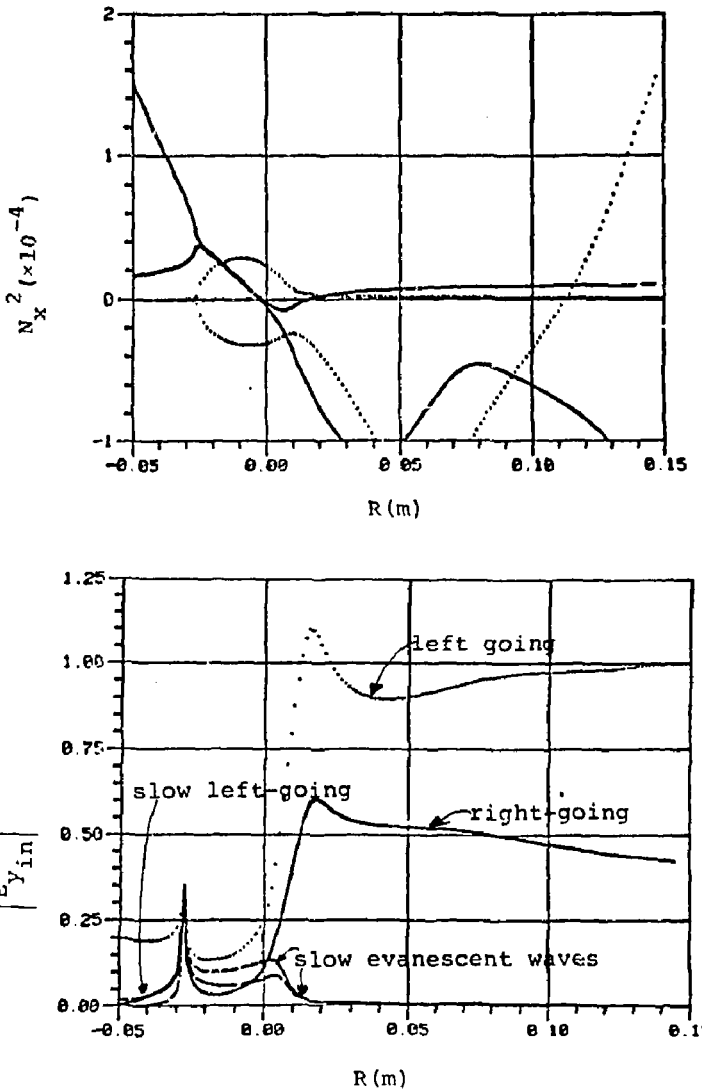
$N_x^2 (\times 10^{-4})$
2
1
0
-1
-0.05
0.00
0.05
0.10
0.15
R(m)
$\left|\frac{E_y}{E_{y_{in}}}\right|$
1.25
1.00
0.75
0.50
0.25
0.00
left going
slow left-going
right-going
slow evanescent waves
-0.05
0.00
0.05
0.10
0.15
R(m)

Fig. 3

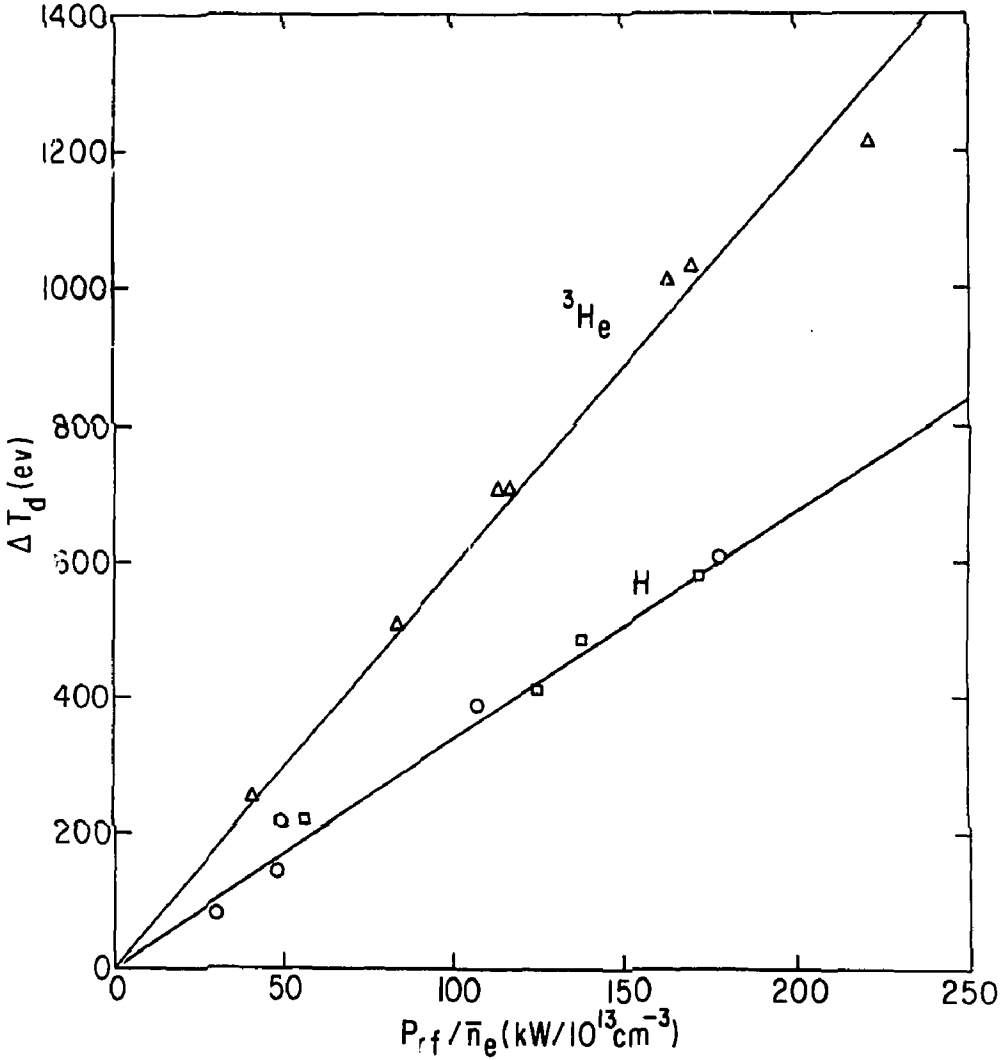


Fig. 4. (PPPL-803428)

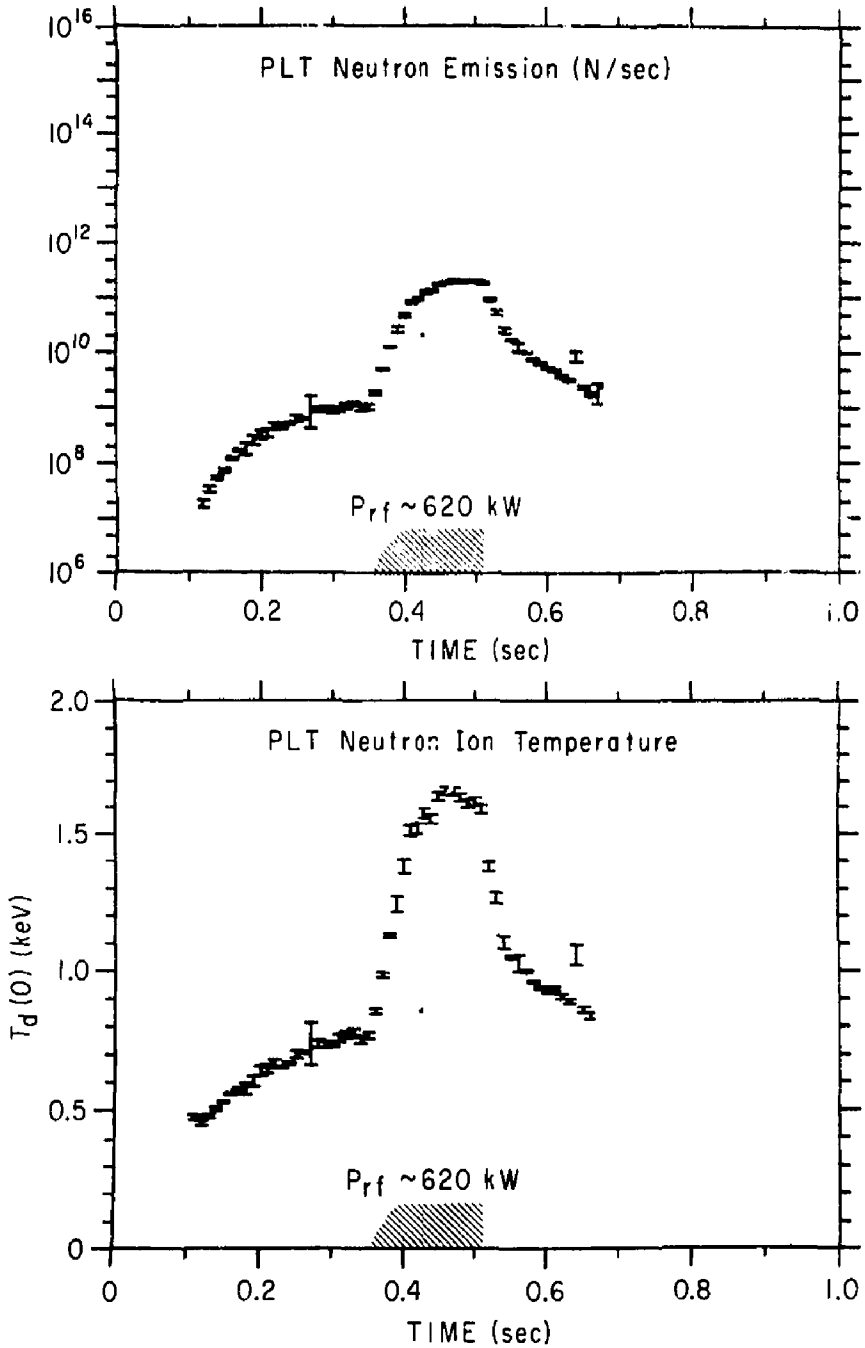


Fig. 5. (PPPL-803429)

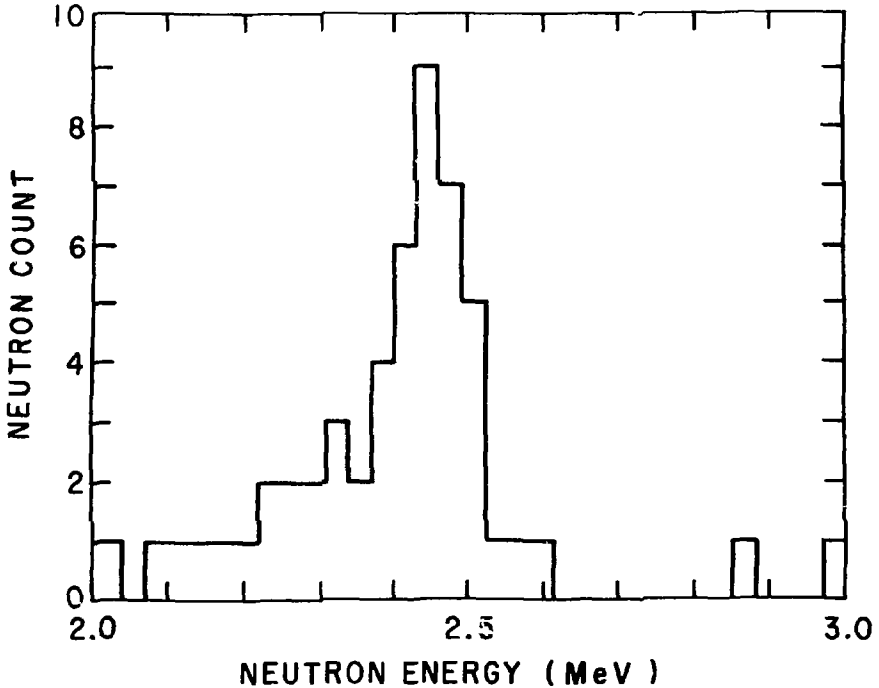


Fig. 6. (PPPL-803431)

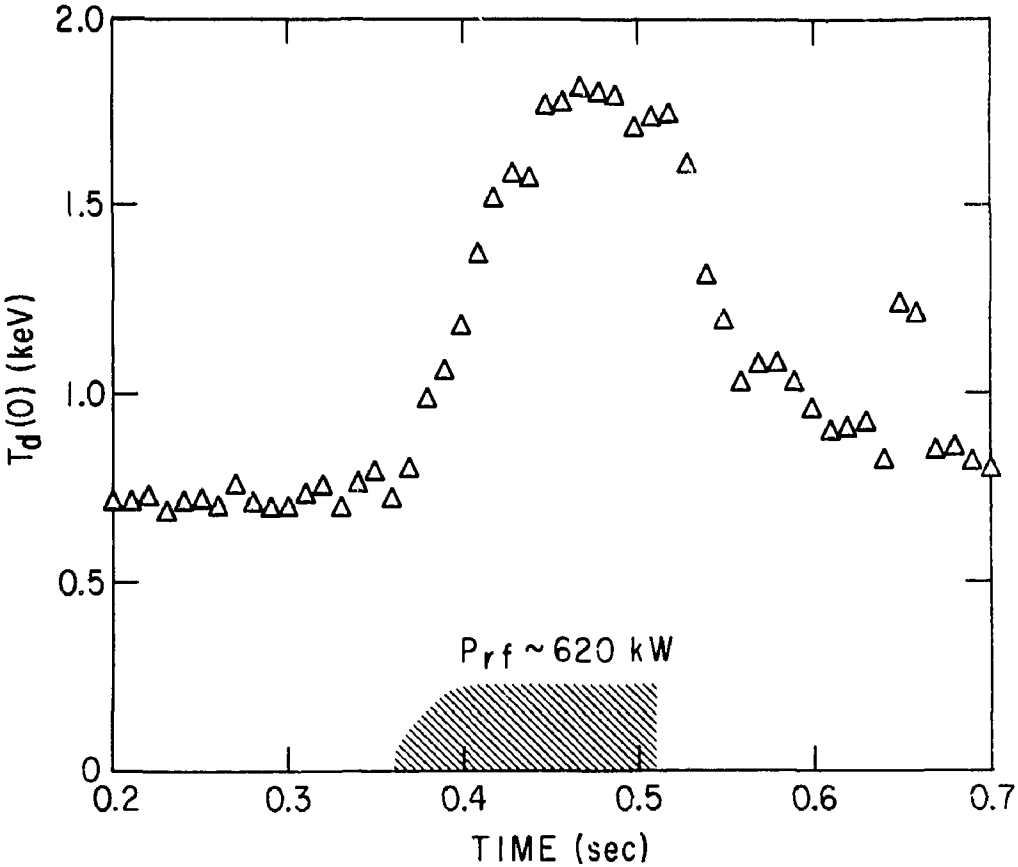


Fig. 7. (PPPL-803433)

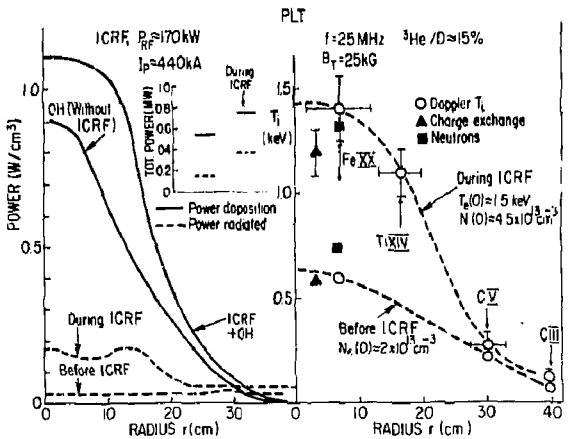


Fig. 8. (PPPL-796406)

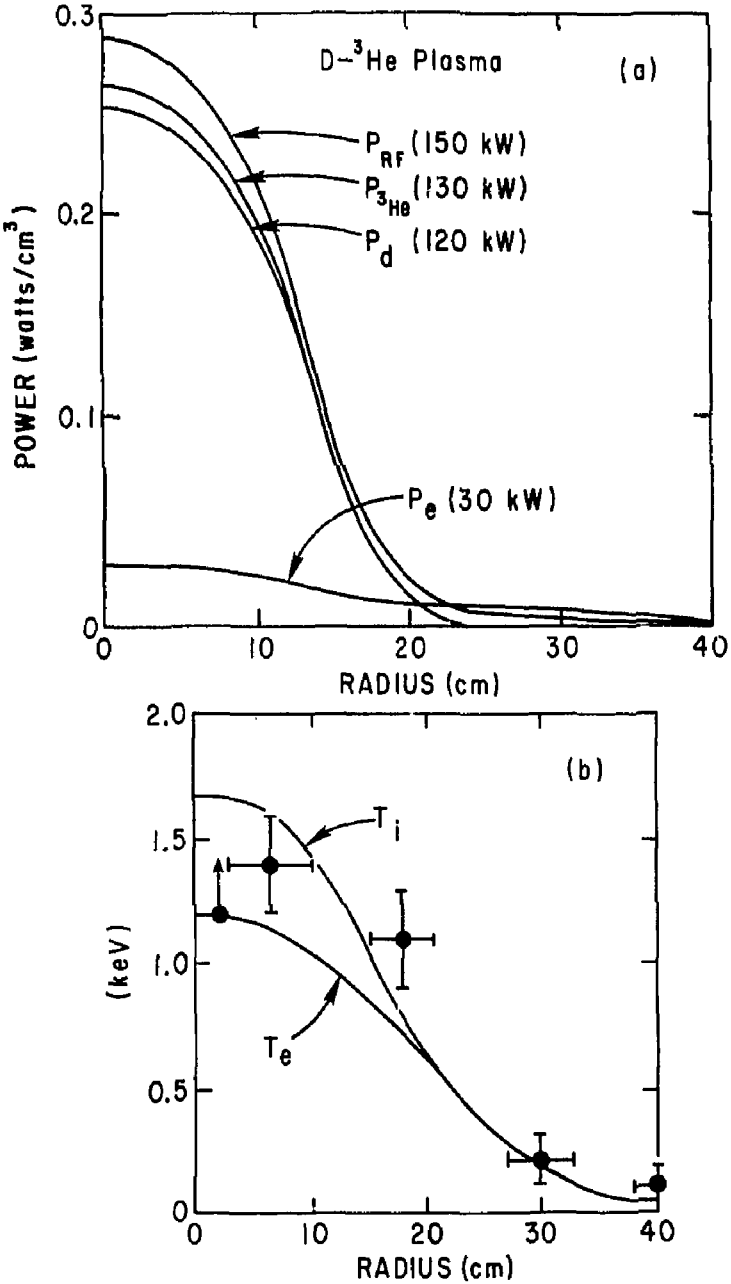


Fig. 9. (PPPL-803432)

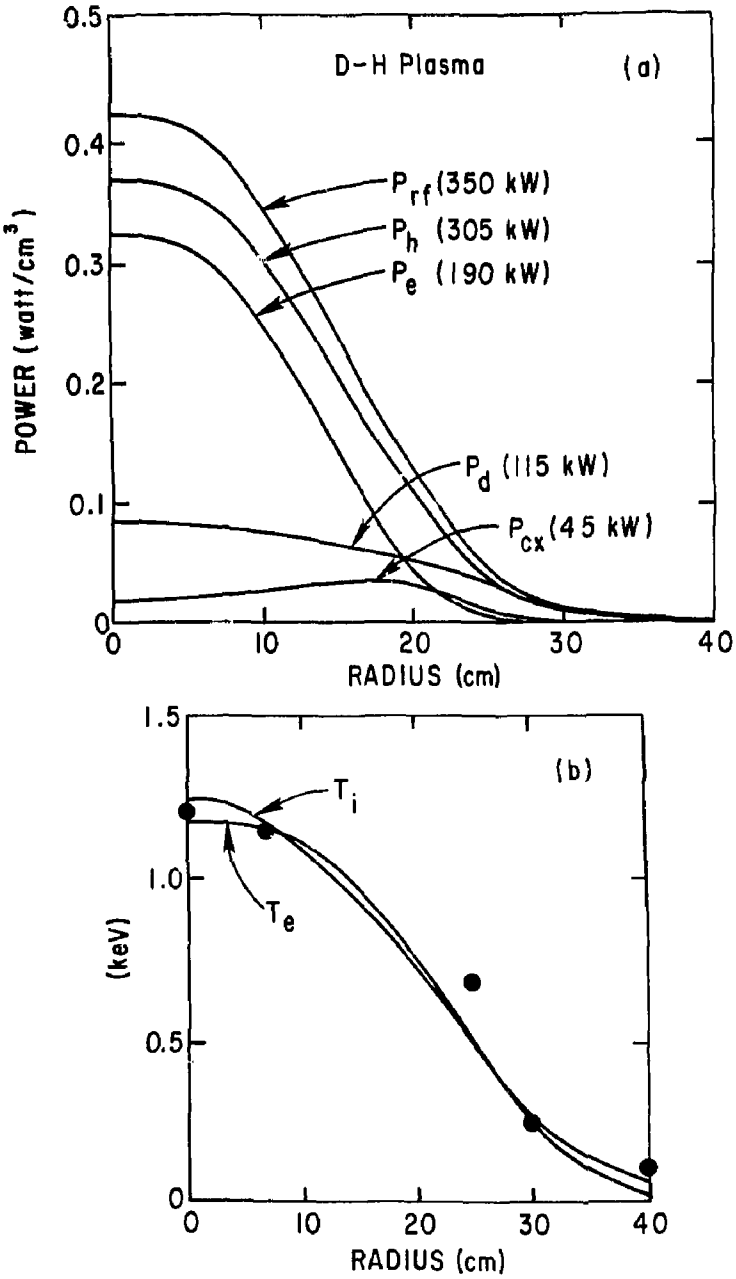


Fig. 9. (PPPL-803425)